Well-Balancing Via Flux Globalization: Applications to Shallow Water Equations with Wet/Dry Fronts

Alina Chertock*, Alexander Kurganov†, Xin Liu‡, Yongle Liu§ and Tong Wu¶

Abstract

We study the flux globalization based central-upwind scheme from [Cheng *et al.*, J. Sci. Comput., 80 (2019), pp. 538–554] for the Saint-Venant system of shallow water equations. We first show that while the scheme is capable of preserving moving-water equilibria, it fails to preserve much simpler "lake-at-rest" steady states. We then modify the computation of the global flux variable and develop a well-balanced scheme, which can accurately handle both still- and moving-water equilibria. In addition, we extend the flux globalization based central-upwind scheme to the case when "dry" and/or "almost dry" areas are present. To this end, we introduce a hybrid approach: we use the flux globalization based scheme inside the "wet" areas only, while elsewhere we apply the central-upwind scheme from [Bollermann *et al.*, J. Sci. Comput., 56 (2013), pp. 267–290], which is designed to accurately capture wet/dry fronts. We illustrate the performance of the proposed schemes on a number of numerical examples.

Key words: flux globalization, central-upwind schemes, well-balanced schemes, "lake-at-rest" steady states, "dry lake" steady states.
AMS subject classification: 76M12, 65M08, 86-08, 35L65.

1 Introduction

We consider one-dimensional (1-D) hyperbolic systems of balance laws, which, in general case, can be written in the following form:

$$\boldsymbol{U}_t + \boldsymbol{f}(\boldsymbol{U})_x = \boldsymbol{S}(\boldsymbol{U}), \tag{1.1}$$

*Department of Mathematics, North Carolina State University, Raleigh, NC 27695, USA; chertock@math.ncsu.edu

†Department of Mathematics, SUSTech International Center for Mathematics and Guangdong Provincial Key Laboratory of Computational Science and Material Design, Southern University of Science and Technology, Shenzhen, 518055, China; alexander@sustech.edu.cn

‡Numerical Environmental Prediction Section, Environment and Climate Change Canada, Dorval, QC, H9P1J3, Canada and Department of Civil Engineering, University of Ottawa, ON, K1N6N5, Canada xliu111@uottawa.ca

§Department of Mathematics, Harbin Institute of Technology, Harbin, 150001, China and Department of Mathematics, Southern University of Science and Technology, Shenzhen, 518055, China; liuyl2017@mail.sustech.edu.cn

¶Department of Mathematics, University of Texas, San Antonio, TX 78249, USA; Tong.wu@utsa.edu

where x is the spatial variable, t is the time, $\boldsymbol{U}$ is the vector of unknowns, $\boldsymbol{f}$ is the flux, and $\boldsymbol{S}$ is the source term. We are interested in development of highly accurate and robust numerical methods for (1.1). It is well-known that such methods should be well-balanced in the sense that they are to be capable of preserving (several physically relevant) steady-state solutions of (1.1) within the machine accuracy. This is especially important since such schemes are typically able to accurately capture small perturbations of the steady states on a coarse computational mesh, which is essential for the scheme to be applicable in many practically relevant applications.

In the past decades, many well-balanced schemes for a wide variety of models described by (1.1) have been proposed. In this paper, we focus on a flux globalization technique recently introduced in [6] and then applied to several shallow water models [4, 11, 12] and the Euler equations with gravitation [5]. In the general setting, the flux globalization approach can be presented as follows: we introduce a global flux variable

$$\boldsymbol{K}(\boldsymbol{U}(x,t)) := \boldsymbol{f}(\boldsymbol{U}(x,t)) + \boldsymbol{R}(\boldsymbol{U}(x,t)), \quad \boldsymbol{R}(\boldsymbol{U}(x,t)) := -\int^{x} \boldsymbol{S}(\boldsymbol{U}(\xi,t))\,\mathrm{d}\xi, \tag{1.2}$$

and use it to rewrite the system of balance laws (1.1) as a system of conservation laws with the global flux:

$$\boldsymbol{U}_t + \boldsymbol{K}(\boldsymbol{U})_x = \boldsymbol{0}. \tag{1.3}$$

The steady-state solution of (1.1) is then given by a very simple equation

$$\boldsymbol{K}(\boldsymbol{U}) = \textbf{Const}, \tag{1.4}$$

and the main idea in the development of a well-balanced scheme for the system (1.3), (1.2) is very simple: use a Riemann-problem-solver-free finite-volume method, which should employ a piecewise polynomial reconstruction of the equilibrium variables $\boldsymbol{K}$. The latter, according to (1.4), are constant at the steady state and thus all of the reconstructed values of $\boldsymbol{K}$ will be constant, which will help the scheme to exactly preserve this steady state.

One of the key issues in designing well-balanced schemes via the flux globalization technique is a proper approximation of the discrete values of the global variables $\boldsymbol{K}$ out of the cell averages of $\boldsymbol{U}$, which are the evolved quantities in finite-volume methods. This requires accurate quadrature rules for the integrals $\boldsymbol{R}$ appearing in (1.2). In particular, in the original paper [6] a generic approach for constructing such quadratures was proposed and later implemented in [4] in the context of the Saint-Venant system of shallow water equations, for which

$$\boldsymbol{U} = \begin{pmatrix} h \\ q \end{pmatrix}, \quad \boldsymbol{f}(\boldsymbol{U}) = \begin{pmatrix} q \\ hu^2 + \dfrac{g}{2}h^2 \end{pmatrix}, \quad \boldsymbol{S}(\boldsymbol{U}) = \begin{pmatrix} 0 \\ -ghB_x - g\dfrac{n^2}{h^{7/3}}|q|q \end{pmatrix}. \tag{1.5}$$

Here, $h(x,t)$ is the water depth, $u(x,t)$ is the velocity, $q(x,t) := h(x,t)u(x,t)$ is the water discharge, $B(x)$ is the bottom topography function, g is the constant gravitational acceleration, and n is the Manning friction coefficient. Using the flux globalization, the shallow water system (1.1), (1.5) can be rewritten in the following equivalent form:

$$\begin{cases} h_t + q_x = 0, \\ q_t + K_x = 0, \end{cases} \tag{1.6}$$

where

$$K := hu^2 + \frac{g}{2}h^2 + R, \tag{1.7}$$

so that K is a global equilibrium variable with

$$R(x,t) := g\int^x \left[h(\xi,t)B_x(\xi) + \frac{n^2}{h^{7/3}(\xi,t)}|q(\xi,t)|q(\xi,t)\right]\mathrm{d}\xi. \tag{1.8}$$

In the absence of dry areas, the system (1.6)–(1.8) admits a family of smooth steady-state solutions satisfying

$$q \equiv \widehat{q} = \text{Const}, \quad K \equiv \widehat{K} = \text{Const}, \quad h > 0. \tag{1.9}$$

One of the particularly simple but practically very important steady-state solutions is the so-called "lake-at-rest" (*still-water*) equilibria with the velocity of the water equal to zero and a flat water surface $w := h + B$:

$$u \equiv 0, \quad w \equiv \widehat{w} = \text{Const}. \tag{1.10}$$

We note that the well-balanced flux globalization based scheme from [4] can preserve moving-water equilibria (1.9) with $q \neq 0$. However, the generic quadrature rule for the global integral R in (1.8) used in this scheme prevents it from preserving the "lake-at-rest" equilibria, and one of the goals of the current paper is to illustrate this. We will also present a way to eliminate this drawback by constructing a proper quadrature rule, which will lead to a flux globalization based scheme capable of preserving both moving- and still-water equilibria.

Another limitation of the flux globalization based scheme from [4] is that it only applies to the "wet" case, in which $h > 0$ for all x. In the presence of "dry" ($h = 0$) or "almost dry" ($h \approx 0$) areas steady-state solutions do not satisfy (1.9) everywhere, that is, steady states consist of several pieces: pieces satisfying (1.9) in the "wet" areas, pieces with $h \equiv 0$, $u \equiv 0$ in the "dry" areas, and wet/dry fronts in the areas separating the "wet" and "dry" parts of the solution. Therefore, the equilibrium variable K cannot be used in the entire computational domain.

The second and the main goal of this paper is to extend the applicability of flux globalization based central-upwind scheme from [4] to the case when "dry" and/or "almost dry" areas are present. In this case, we identify the wet/dry fronts and use the global fluxes (1.7) inside the "wet" areas only, while in the "dry" areas and near the wet/dry fronts, we implement the central-upwind scheme from [2], which is based on a special piecewise linear reconstruction of the water surface w in those areas. We prove that the resulting scheme is capable of exactly preserving "lake-at-rest" steady states in the presence of "dry" or "almost dry" areas.

The paper is organized as follows. §2 is devoted to the flux globalization approach in the fully flooded case, that is, when the bottom topography is fully submerged in the entire computational domain. In §2.1, we give an overview of the flux globalization based central-upwind scheme from [4]. In §2.2, we demonstrate the insufficient flux-source balancing in this scheme, which prevents it from being capable of exactly preserving "lake-at-rest" steady states. In §2.3, we introduce a new well-balanced computation of the global variables, which helps to make the modified flux globalization based central-upwind scheme to be capable of exactly preserving both moving- and still-water equilibria. In §2.4, we test the schemes on two numerical examples and illustrate that the modified scheme clearly outperforms the scheme from [4]. In §3, we study the situation when "dry" and/or "almost dry" areas are present and develop a new hybrid well-balanced central-upwind scheme capable of accurately handling wet/dry fronts. Our hybrid strategy on a hybrid

piecewise linear reconstruction, summarized in §3.1, and different time evolution inside and outside the "wet" areas, as described in §3.2. The performance of the proposed hybrid scheme is illustrated on two numerical examples in §3.3.

2 Flux Globalization in the Fully Flooded Case

We split the computational domain into the uniform (for simplicity) cells $C_j := [x_{j-\frac{1}{2}}, x_{j+\frac{1}{2}}]$, $j = j_\ell, \ldots, j_r$ with $x_{j+\frac{1}{2}} - x_{j-\frac{1}{2}} \equiv \Delta x$. We assume that at a certain time level t, the computed solution realized in terms of its cell averages

$$\overline{\boldsymbol{U}}_j(t) :\approx \frac{1}{\Delta x}\int\limits_{C_j} \boldsymbol{U}(x,t)\,\mathrm{d}x,$$

is available. We also follow the approach introduced in [13] and replace the bottom topography function $B(x)$ with its continuous piecewise linear approximation

$$\widetilde{B}(x) = B_{j-\frac{1}{2}} + \frac{B_{j+\frac{1}{2}} - B_{j-\frac{1}{2}}}{\Delta x}\big(x - x_{j-\frac{1}{2}}\big), \quad x \in C_j,$$

where

$$B_{j+\frac{1}{2}} := \frac{B(x_{j+\frac{1}{2}}+0) + B(x_{j+\frac{1}{2}}-0)}{2},$$

which reduces to $B_{j+\frac{1}{2}} := B(x_{j+\frac{1}{2}})$ if B is continuous at $x = x_{j+\frac{1}{2}}$. We then introduce the following notations:

$$B_j := \widetilde{B}(x_j) = \frac{B_{j+\frac{1}{2}} + B_{j-\frac{1}{2}}}{2}, \quad (B_x)_j := \widetilde{B}_x(x_j) = \frac{B_{j+\frac{1}{2}} - B_{j-\frac{1}{2}}}{\Delta x}. \tag{2.1}$$

In this section, we assume that no "dry" or "almost dry" areas are present and that all of the computational cells remain fully flooded at all times. The definition of fully flooded, dry and partially flooded cells are given by

Definition 2.1 *We say that the cell C_j at time t is:*

(i) fully flooded *if*

$$\overline{h}_j(t) > \varepsilon \quad \textit{and} \quad \overline{h}_j(t) + B_j \geq \max\left(B_{j-\frac{1}{2}}, B_{j+\frac{1}{2}}\right), \tag{2.2}$$

where ε is a small positive number chosen in such a way that the amount of water present in cell j can be considered as negligibly small according to the scales of the studied problem;

(ii) dry *if*

$$\overline{h}_j(t) \leq \varepsilon; \tag{2.3}$$

(iii) partially flooded *if neither (2.2) or (2.3) is satisfied.*

Note that equation (2.2) can be equivalently rewritten as

$$\overline{h}_j(t) \geq \frac{\Delta x}{2}|(B_x)_j|.$$

We also note that $\overline{\boldsymbol{U}}_j$, $\overline{h}_j$ as well as many other indexed quantities below depend on t, but from now on we will omit this dependence for the sake of brevity.

2.1 Flux Globalization Based Central-Upwind Scheme from [4]: An Overview

In this section, we briefly review the second-order semi-discrete central-upwind scheme based on the flux globalization technique for the 1-D Saint-Venant system of shallow water equations (1.6)–(1.8).

The solution is evolved in time according to the following semi-discretization:

$$\frac{\mathrm{d}}{\mathrm{d}t}\overline{\boldsymbol{U}}_j=-\frac{\boldsymbol{H}_{j+\frac12}-\boldsymbol{H}_{j-\frac12}}{\Delta x},\tag{2.4}$$

where $\boldsymbol{H}_{j+\frac12}=\big(H^{(1)}_{j+\frac12},H^{(2)}_{j+\frac12}\big)^\top$ are the central-upwind numerical fluxes from [10]:

$$\begin{aligned}H^{(1)}_{j+\frac12}&=\frac{a^+_{j+\frac12}q^-_{j+\frac12}-a^-_{j+\frac12}q^+_{j+\frac12}}{a^+_{j+\frac12}-a^-_{j+\frac12}}+\frac{a^+_{j+\frac12}a^-_{j+\frac12}}{a^+_{j+\frac12}-a^-_{j+\frac12}}\Big(h^+_{j+\frac12}-h^-_{j+\frac12}\Big),\\ H^{(2)}_{j+\frac12}&=\frac{a^+_{j+\frac12}K^-_{j+\frac12}-a^-_{j+\frac12}K^+_{j+\frac12}}{a^+_{j+\frac12}-a^-_{j+\frac12}}+\frac{a^+_{j+\frac12}a^-_{j+\frac12}}{a^+_{j+\frac12}-a^-_{j+\frac12}}\Big(q^+_{j+\frac12}-q^-_{j+\frac12}\Big).\end{aligned}\tag{2.5}$$

Here, $h^\pm_{j+\frac12}$, $q^\pm_{j+\frac12}$ and $K^\pm_{j+\frac12}$ are the left/right-sided point values of h, q and K at the cell interface $x=x_{j+\frac12}$ (for the details, see below), and $a^\pm_{j+\frac12}$ are the one-sided local propagation speeds, which can be estimated by

$$\begin{aligned}a^+_{j+\frac12}&=\max\Big\{u^-_{j+\frac12}+\sqrt{gh^-_{j+\frac12}},\,u^+_{j+\frac12}+\sqrt{gh^+_{j+\frac12}},\,0\Big\},\\ a^-_{j+\frac12}&=\min\Big\{u^-_{j+\frac12}-\sqrt{gh^-_{j+\frac12}},\,u^+_{j+\frac12}-\sqrt{gh^+_{j+\frac12}},\,0\Big\}.\end{aligned}$$

In order to complete the construction of the scheme, one needs to provide an algorithm for computing the point values $h^\pm_{j+\frac12}$, $q^\pm_{j+\frac12}$ and $K^\pm_{j+\frac12}$ out of the available cell averages $\{\overline{h}_j\}$ and $\{\overline{q}_j\}$. As mentioned in the Introduction, the key point is to use a piecewise linear reconstruction of the equilibrium variables q and K. According to [4], one can proceed as follows. We first use the midpoint rule to compute the integral in (1.8) with the lower integration limit set to be $x_{j_\ell-\frac12}$. This results in the following recursive formula for the point values of the global variable R at the cell interfaces $x=x_{j+\frac12}$:

$$R_{j_\ell-\frac12}:=0,\quad R_{j+\frac12}=R_{j-\frac12}+g\Delta x\bigg(\overline{h}_j(B_x)_j+\frac{n^2}{\overline{h}_j^{7/3}}|\overline{q}_j|\overline{q}_j\bigg),\quad j=j_\ell,\ldots,j_r.\tag{2.6}$$

After that, the point values of R at the cell centers $x=x_j$ were computed in [4] using a straightforward approach, namely, by setting

$$R_j=\frac12\big(R_{j+\frac12}+R_{j-\frac12}\big),\quad j=j_\ell,\ldots,j_r.\tag{2.7}$$

Next, from the definition of K in formula (1.7), we obtain the point values of K at the cell centers $x=x_j$:

$$K_j=\frac{\overline{q}_j^2}{\overline{h}_j}+\frac{g}{2}\overline{h}_j^2+R_j,\tag{2.8}$$

which are used, along with the cell averages $\bar{q}_j$, to compute the one-sided point values of q and K at the cell interfaces $x = x_{j+\frac{1}{2}}$:

$$\begin{aligned} &q^-_{j+\frac{1}{2}} := \widetilde{q}(x_{j+\frac{1}{2}}-0) = \bar{q}_j + \frac{\Delta x}{2}(q_x)_j, \qquad q^+_{j+\frac{1}{2}} := \widetilde{q}(x_{j+\frac{1}{2}}+0) = \bar{q}_{j+1} - \frac{\Delta x}{2}(q_x)_{j+1},\\ &K^-_{j+\frac{1}{2}} := \widetilde{K}(x_{j+\frac{1}{2}}-0) = K_j + \frac{\Delta x}{2}(K_x)_j, \quad K^+_{j+\frac{1}{2}} := \widetilde{K}(x_{j+\frac{1}{2}}+0) = K_{j+1} - \frac{\Delta x}{2}(K_x)_{j+1}. \end{aligned} \tag{2.9}$$

Here, $\widetilde{q}$ and $\widetilde{K}$ are the piecewise linear reconstructions,

$$\widetilde{q}(x) = \bar{q}_j + (q_x)_j(x-x_j), \quad \widetilde{K}(x) = K_j + (K_x)_j(x-x_j), \quad x \in C_j, \tag{2.10}$$

with the slopes $(q_x)_j$ and $(K_x)_j$ computed using the generalized minmod limiter [15, 17, 18]:

$$\begin{aligned} &(q_x)_j = \text{minmod}\left(\theta\,\frac{\bar{q}_{j+1}-\bar{q}_j}{\Delta x}, \frac{\bar{q}_{j+1}-\bar{q}_{j-1}}{2\Delta x}, \theta\,\frac{\bar{q}_j-\bar{q}_{j-1}}{\Delta x}\right),\\ &(K_x)_j = \text{minmod}\left(\theta\,\frac{K_{j+1}-K_j}{\Delta x}, \frac{K_{j+1}-K_{j-1}}{2\Delta x}, \theta\,\frac{K_j-K_{j-1}}{\Delta x}\right), \end{aligned} \qquad \theta \in [1,2], \tag{2.11}$$

where the minmod function is defined by

$$\text{minmod}(z_1, z_2, \ldots) := \begin{cases} \min(z_1, z_2, \ldots), & \text{if } \ z_i > 0 \ \ \forall i,\\ \max(z_1, z_2, \ldots), & \text{if } \ z_i < 0 \ \ \forall i,\\ 0, & \text{otherwise,} \end{cases}$$

and the parameter θ is used to control the amount of the numerical dissipation—larger values of θ correspond to sharper, but more dispersive reconstructions. In all of the numerical examples reported below, we have taken $\theta = 1.3$.

Finally, equipped with the point values $q^\pm_{j+\frac{1}{2}}$ and $K^\pm_{j+\frac{1}{2}}$, we need to approximate the corresponding water depth values. To this end, we solve the following cubic equations for $h^\pm_{j+\frac{1}{2}}$:

$$K^+_{j+\frac{1}{2}} = \frac{\big(q^+_{j+\frac{1}{2}}\big)^2}{h^+_{j+\frac{1}{2}}} + \frac{g}{2}\big(h^+_{j+\frac{1}{2}}\big)^2 + R_{j+\frac{1}{2}}, \quad K^-_{j+\frac{1}{2}} = \frac{\big(q^-_{j+\frac{1}{2}}\big)^2}{h^-_{j+\frac{1}{2}}} + \frac{g}{2}\big(h^-_{j+\frac{1}{2}}\big)^2 + R_{j+\frac{1}{2}}. \tag{2.12}$$

The details on solving these equations can be found in [4].

Remark 2.2 *The system of ODEs (2.4) has to be solved by a stable and accurate ODE solver. In all of the numerical experiments reported below, we have used the three-stage third-order strong stability preserving (SSP) Runge-Kutta method [8, 9] with the time step selected adaptively using the CFL number 0.5.*

2.2 Insufficient Flux-Source Balancing in the Scheme from [4]

It was demonstrated in [4] that the central-upwind scheme described in §2.1 can preserve the moving-water equilibria given by (1.9). The question we investigate in this section is whether that scheme is also capable of preserving the "lake-at-rest" (still water) equilibria given by (1.10) as

well. It is easy to check that on the continuous level (1.9) reduces to (1.10) when $q \equiv 0$. This is, however, not true on the discrete level as we show below.

Let us consider the discrete data, which is at the "lake-at-rest" steady state satisfying

$$\overline{q}_j = u_j \equiv 0, \quad \overline{h}_j = \widehat{w} - B_j, \quad \text{for all } j, \tag{2.13}$$

where $\widehat{w}$ is a given constant. Our goal is to check whether (2.13) implies that $K_j = K_{j+1}$ for all j. According to (2.7), (2.8), we obtain that for the "lake-at-rest" data

$$K_j = \frac{g}{2}\overline{h}_j^2 + \frac{1}{2}\big(R_{j+\frac{1}{2}} + R_{j-\frac{1}{2}}\big), \quad K_{j+1} = \frac{g}{2}\overline{h}_{j+1}^2 + \frac{1}{2}\big(R_{j+\frac{3}{2}} + R_{j+\frac{1}{2}}\big).$$

Then, subtracting K_j from K_{j+1} and using (2.6) and (2.13) results in

$$\begin{aligned}
K_{j+1} - K_j &= \frac{g}{2}\big(\overline{h}_{j+1}^2 - \overline{h}_j^2\big) + \frac{1}{2}\big(R_{j+\frac{3}{2}} - R_{j-\frac{1}{2}}\big)\\
&= \frac{g}{2}\big(\overline{h}_{j+1}^2 - \overline{h}_j^2\big) + \frac{g}{2}\Big(\overline{h}_{j+1}\big(B_{j+\frac{3}{2}} - B_{j+\frac{1}{2}}\big) + \overline{h}_j\big(B_{j+\frac{1}{2}} - B_{j-\frac{1}{2}}\big)\Big)\\
&= \frac{g}{2}\Big((\widehat{w} - B_{j+1})^2 - (\widehat{w} - B_j)^2\Big)\\
&+ \frac{g}{2}\Big((\widehat{w} - B_{j+1})\big(B_{j+\frac{3}{2}} - B_{j+\frac{1}{2}}\big) + (\widehat{w} - B_j)\big(B_{j+\frac{1}{2}} - B_{j-\frac{1}{2}}\big)\Big).
\end{aligned}$$

Finally, we use the first equality in (2.1) and end up with

$$K_{j+1} - K_j = -\frac{g}{4}\big(B_{j+\frac{3}{2}} - B_{j-\frac{1}{2}}\big)\big(B_{j+\frac{3}{2}} - 2B_{j+\frac{1}{2}} + B_{j-\frac{1}{2}}\big),$$

which might obviously be not zero for a nonflat nonlinear bottom topography B.

We stress that since K_j will not necessarily be constant for all j, the numerical flux difference $H^{(2)}_{j+\frac{1}{2}} - H^{(2)}_{j-\frac{1}{2}}$ will not vanish for some j, and thus the right-hand side (RHS) of (2.4) will not be identically equal to zero, which will prevent the scheme from being well-balanced.

The main reason the scheme from [4] does not preserve the discrete "lake-at-rest" steady states (2.13) is related to the way the discrete values of the global vabiable R_j are evaluated in (2.7). In the next section, we propose an alternative way, which would lead to another version of the flux globalization based central-upwind scheme, which is capable of preserving both moving- and still-water equilibria.

2.3 Well-Balanced Computation of the Global Variables

As one can see from the computation in §2.2, the lack of balancing in the original scheme from [4] is caused by the way the values R_j are computed in (2.7). We propose to modify this computation in the following recursive way.

We begin by approximating the global variable R at the first cell on the left of the computational domian, that is, at $x = x_{j_\ell}$. Namely, we need to evaluate

$$R_{j_\ell} = R_{j_\ell-\frac{1}{2}} + \int\limits_{x_{j_\ell-\frac{1}{2}}}^{x_{j_\ell}} \Big(ghB_x + g\frac{n^2}{h^{7/3}}|q|q\Big)\mathrm{d}x = \int\limits_{x_{j_\ell-\frac{1}{2}}}^{x_{j_\ell}} \Big(ghB_x + g\frac{n^2}{h^{7/3}}|q|q\Big)\mathrm{d}x. \tag{2.14}$$

Our goal is to make sure that the quadrature for the intergral on the RHS of (2.14) is exact when the data correspond to the "lake-at-rest" steady state (2.13), that is, when $\overline{q}_{j_\ell}=0$ and $\overline{h}_{j_\ell}=\widehat{w}-B_{j_\ell}$. To this end, we replace the functions B, h and q in this intergral with

$$\widetilde{B}_{j_\ell}(x)=B_{j_\ell-\frac{1}{2}}+(B_x)_{j_\ell}(x-x_{j_\ell}),\quad \widetilde{h}_{j_\ell}(x)=\overline{h}_{j_\ell}+\frac{1}{2}\big(B_{j_\ell-\frac{1}{2}}+B_{j_\ell+\frac{1}{2}}\big)-\widetilde{B}_{j_\ell}(x)\quad\text{and}\quad \widetilde{q}_{j_\ell}(x)=\overline{q}_{j_\ell},$$

respectively, and apply the trapezoidal rule to obtain

$$\begin{aligned}R_{j_\ell}&\approx\int\limits_{x_{j_\ell-\frac{1}{2}}}^{x_{j_\ell}}\Big(g\widetilde{h}_{j_\ell}(x)(B_x)_{j_\ell}+g\frac{n^2}{\big(\widetilde{h}_{j_\ell}(x)\big)^{7/3}}|\widetilde{q}_{j_\ell}(x)|\widetilde{q}_{j_\ell}(x)\Big)\mathrm{d}x\\&\approx\frac{g\Delta x}{2}\left[(B_x)_{j_\ell}\frac{\widetilde{h}_{j_\ell}(x_{j_\ell-\frac{1}{2}})+\widetilde{h}_{j_\ell}(x_{j_\ell})}{2}+\frac{n^2}{2}|\overline{q}_{j_\ell}|\overline{q}_{j_\ell}\left\{\frac{1}{\big(\widetilde{h}_{j_\ell}(x_{j_\ell-\frac{1}{2}})\big)^{7/3}}+\frac{1}{\big(\widetilde{h}_{j_\ell}(x_{j_\ell})\big)^{7/3}}\right\}\right]\\&=\frac{g\Delta x}{2}\left[(B_x)_{j_\ell}\Big(\overline{h}_{j_\ell}+\frac{\Delta x}{4}(B_x)_{j_\ell}\Big)+\frac{n^2}{2}|\overline{q}_{j_\ell}|\overline{q}_{j_\ell}\left\{\frac{1}{\big(\overline{h}_{j_\ell}+\frac{\Delta x}{2}(B_x)_{j_\ell}\big)^{7/3}}+\frac{1}{\big(\overline{h}_{j_\ell}\big)^{7/3}}\right\}\right].\end{aligned}\tag{2.15}$$

We then follow the approach proposed in [11,12,14], and use a special second-order quadrature rule to obtain the following recursive formula:

$$\begin{aligned}R_{j+1}&=R_j+\int\limits_{x_j}^{x_{j+1}}\Big(ghB_x+g\frac{n^2}{h^{7/3}}|q|q\Big)\mathrm{d}x\\&=R_j+\frac{g}{2}\big(\overline{h}_{j+1}+\overline{h}_j\big)\big(B_{j+1}-B_j\big)+\frac{gn^2\Delta x}{2}\left\{\frac{|\overline{q}_{j+1}|\overline{q}_{j+1}}{\big(\overline{h}_{j+1}\big)^{7/3}}+\frac{|\overline{q}_j|\overline{q}_j}{\big(\overline{h}_j\big)^{7/3}}\right\},\quad j=j_\ell,\ldots,j_r-1.\end{aligned}\tag{2.16}$$

We now verify that if (2.7) is replaced with (2.15), (2.16), the resulting scheme will preserve the "lake-at-rest" steady states satisfying (2.13). To this end, as in §2.2 we assume that the data are at the discrete equilibrium (2.13) and we need to show that in this case, $K_j=K_{j+1}$ for all j. Indeed, we have

$$\begin{aligned}K_{j+1}-K_j&=\frac{g}{2}\big(\overline{h}_{j+1}^2-\overline{h}_j^2\big)+R_{j+1}-R_j=\frac{g}{2}\big(\overline{h}_{j+1}^2-\overline{h}_j^2\big)+\frac{g}{2}\big(\overline{h}_{j+1}+\overline{h}_j\big)\big(B_{j+1}-B_j\big)\\&=\frac{g}{2}\big(\overline{h}_{j+1}+\overline{h}_j\big)\big(\overline{h}_{j+1}+B_{j+1}-(\overline{h}_j+B_j)\big)=\frac{g}{2}(\overline{h}_{j+1}+\overline{h}_j)(\widehat{w}-\widehat{w})=0.\end{aligned}$$

2.4 Numerical Example

In this section, we demonstrate that the proposed flux globalization based central-upwind scheme clearly outperforms the scheme from [4].

Example 1—"Lake-at-Rest" Steady State

We first consider the "lake-at-rest" steady state subject to the initial data

$$h(x,0)=3-B(x),\quad q(x,0)\equiv0,\tag{2.17}$$

which are prescribed in the computational domain $[-1,1]$ supplemented with the free boundary conditions. The bottom topography contains a hump located between $x=0.1$ and $x=0.3$:

$$B(x)=\begin{cases}1.25\big[\cos(10\pi(x-0.2))+1\big], & \text{if } 0.1\le x\le 0.3,\\ 0, & \text{otherwise.}\end{cases}$$

We take the gravitational constant $g=9.8$, the Manning friction coefficient $n=0.05$ and compute the numerical solutions until the final time $t=10$ with 50 uniform cells using both the proposed scheme and the scheme from [4]. The obtained discrete L^1- and L^∞-errors are reported in Table 2.1. As one can clearly see, the proposed scheme preserves the "lake-at-rest" steady state within a machine accuracy while the errors in the scheme from [4] are quite large as the scheme from [4] cannot preserve "lake-at-rest" steady states.

	L^1-error in h	L^∞-error in h	L^1-error in q	L^∞-error in q
Proposed scheme	6.13e-16	8.88e-16	9.51e-14	6.70e-14
Scheme from [4]	8.80e-3	8.68e-2	8.21e-6	4.10e-6

Table 2.1: Example 1: L^1- and L^∞-errors in the water depth h and discharge q.

Example 2—Small Perturbation of the "Lake-at-Rest" Steady State

In the second example, we use the same data as in Example 1, but add a small perturbation to the steady state (2.17) and consider the following initial data:

$$h(x,0)=3-B(x)+\begin{cases}10^{-5}, & \text{if } -0.2\le x\le -0.1,\\ 0, & \text{otherwise,}\end{cases}\qquad q(x,0)\equiv 0.$$

The difference between the computed $h(x,t)$ and the background stationary water depth $h_{\rm eq}(x):=3-B(x)$ computed using a uniform mesh with 100 cells at times $t=0.02$, 0.06 and 0.08 is plotted in Figure 2.1. As one can see, the evolution of the small perturbation is captured very well by the proposed scheme: at $t=0.02$, the perturbation splits into two waves propagating in the opposite directions; at $t=0.06$, the right-going wave passes over the bottom hump and its magnitude increases; at $t=0.08$, the right-going wave passes over the hump, its magnitude decreases and a small reflected wave is generated. At the same time, none of these phenomena can be captured by the scheme from [4], whose truncation error dominates the waves to be captured on the coasre grid selected.

In order to futher demonstrate the importance of an improved well-balanced property of the proposed scheme, we compute the solutions at the same times using the two studied schemes, but on a substantially finer mesh consisting of 5000 uniform cells. The obtained differernces $h(x,t)-h_{\rm eq}(x)$ are plotted in Figure 2.2, where one can observe a much higher resolution achieved by the proposed scheme. At the same time, the scheme from [4] can accurately capture the left-going wave only, whereas the right-going wave, which interacts with the nonflat bottom topography, is still dominated by the spurious waves whose magnitude is proportional to the size of truncation error.

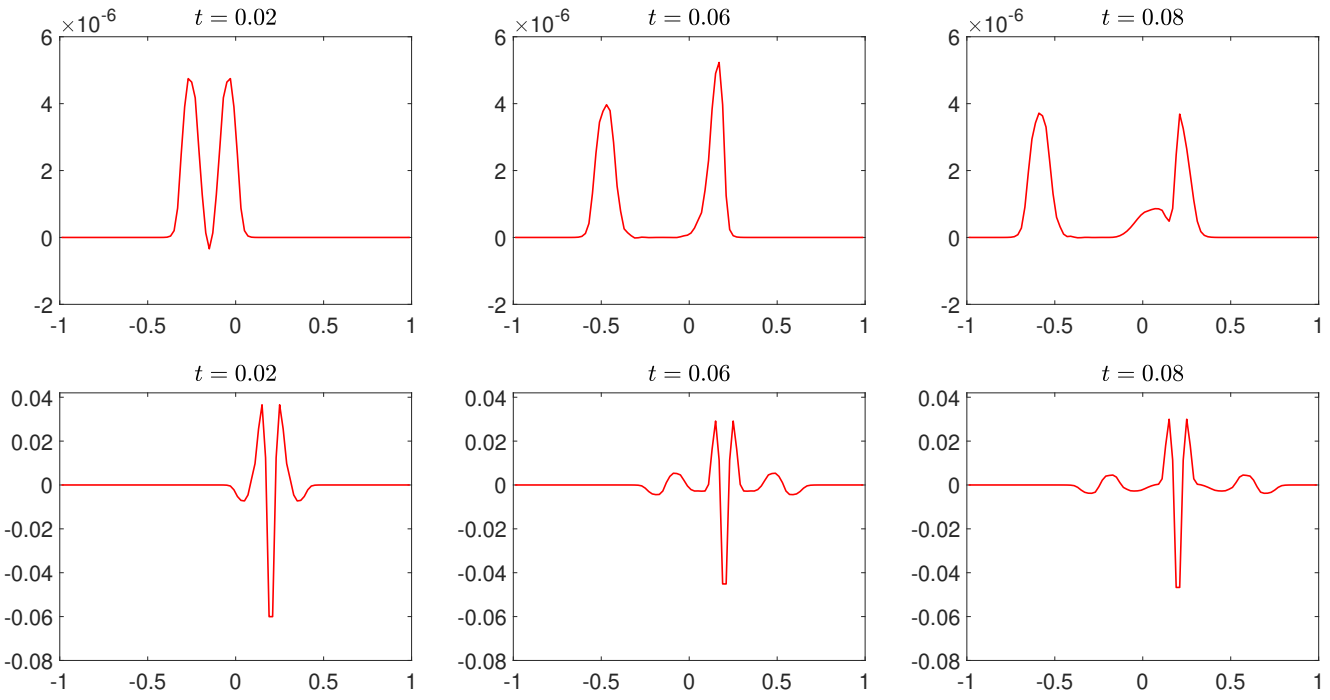

Figure 2.1: Example 1: Time snapshots of the difference $h(x,t) - h_{\rm eq}(x)$, computed by the proposed scheme (top row) and by the scheme from [4] (bottom row) using a coarse mesh with 100 cells.

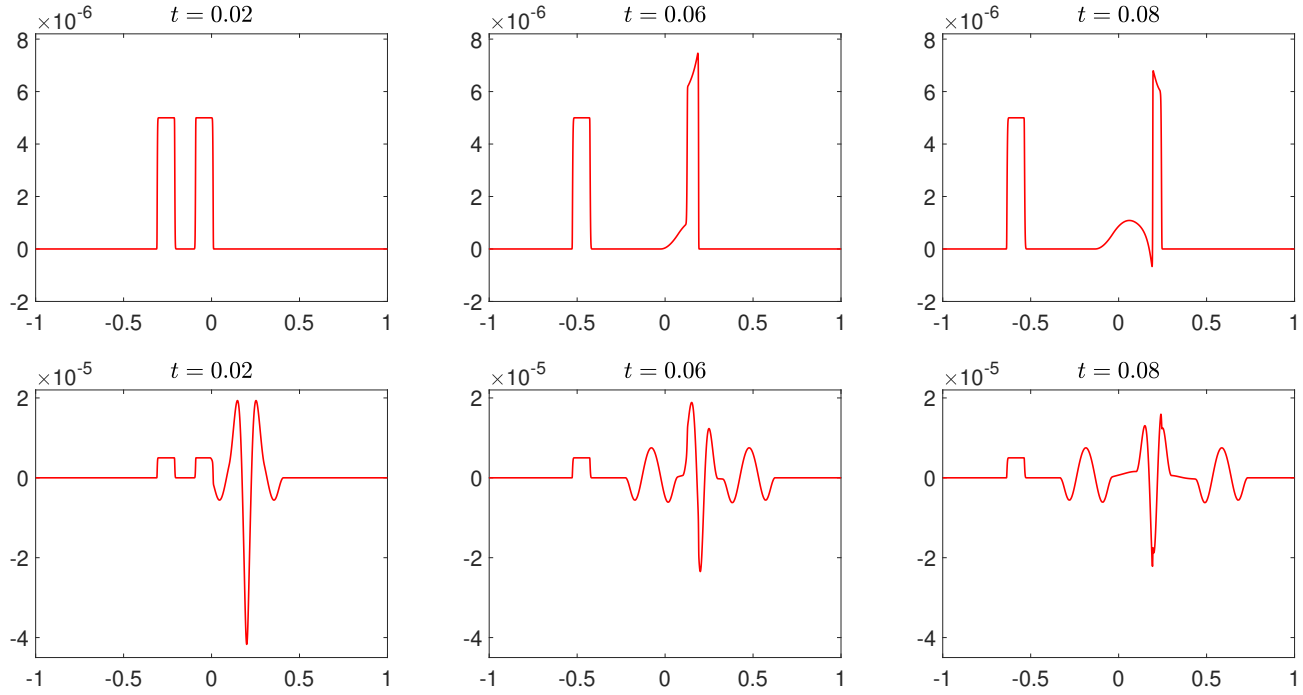

Figure 2.2: Example 1: Same as Figure 2.1 but using a substantially finer mesh with 5000 cells.

3 New Hybrid Well-Balanced Central-Upwind Scheme for Shallow Water Equations with Wet/Dry Fronts

Recall that in §2, the discussion was restricted to the case when all of the computational cells are fully flooded, that is, they satisfy Definition 2.1. We now turn our attention to the case

when the computational domain contains "dry" and/or "almost dry" areas. This is practically important as it corresponds to the presence of islands and/or shore areas, and our goal is to extend the well-balanced flux globalization based central-upwind scheme presented in §2 to such cases. Specifically, we derive the scheme, which can preserve not only "lake-at-rest" steady states (2.13), but also "dry lake" states as well as their combinations. The "dry lake" equilibrium is defined as

$$\overline{q}_j = u_j \equiv 0, \quad \overline{h}_j = 0, \quad \text{for all } j.$$

In Figure 3.1, we present a typical steady-state setting with "lake-at-rest" and "dry lake" states combined. Here, we assume that the cells are numbered as follows: cells $C_{j_\ell}, \ldots, C_{j_r}$ are fully flooded, while cells C_j with $j < j_\ell$ and $j > j_r$ are either partially flooded or dry.

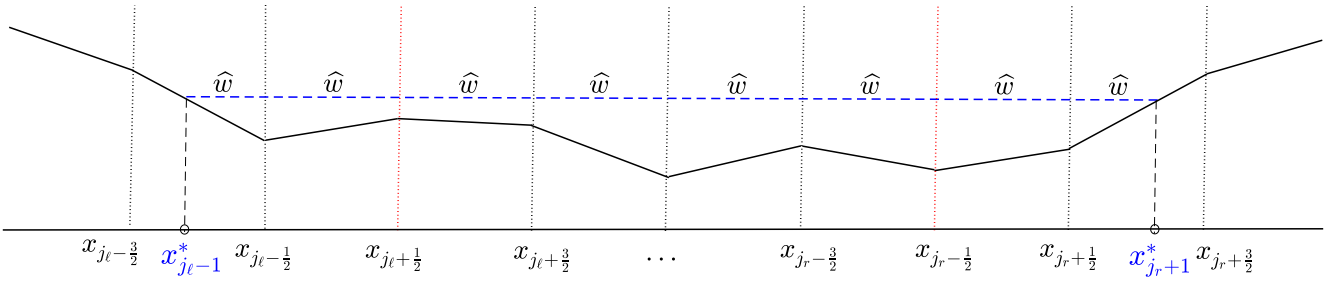

Figure 3.1: Sketch of the combination of the "lake-at-rest" and "dry lake" steady states. Cells $C_{j_\ell-1}$ and C_{j_r+1} are partially flooded; cells $C_{j_\ell}, \ldots, C_{j_r}$ are fully flooded; other cells are dry.

First of all, we note that the Manning friction term should be modified in "dry" and "almost dry" ares, and therefore we consider only the frictionless version of the system (1.6)–(1.8) with $n = 0$ in the current section. Second, we would like to draw the reader's attention to the fact that the global flux K is not constant at the studied combined steady states as in the "dry" areas on the left the values of K will simply vanish. We will therefore introduce all of the global variables inside the "wet" areas only, and in the case when there are multiple "wet" areas, one has to introduce its own set of global variables in each of such areas. Third, we follow [2] and introduce the free surface in cell C_j (denoted by w_j), which represents the average total water level in (the flooded parts of) this cell assuming that the water is at rest; see Figure 3.2, where we sketch the partially flooded cell $C_{j_\ell-1}$ and a typical fully flooded cell C_j. We always choose w_j such that the area enclosed between the line with height w_j and the bottom line $\widetilde{B}_j$ equals the amount of water given by $\Delta x \cdot \overline{h}_j$. The resulting area is either a triangle (in a partially flooded cell; see Figure 3.2 (left)) or a trapezoid (in a fully flooded cell; see Figure 3.2 (right)). So, if the cell C_j is fully flooded, the free surface $\Psi_j(x)$ is defined as

$$\Psi_j(x) = w_j, \quad x \in C_j,$$

otherwise the free surface is a continuous piecewise linear function. Assuming that as in Figure 3.2 (left) $B_{j-\frac{1}{2}} > B_{j+\frac{1}{2}}$ (the opposite case $B_{j-\frac{1}{2}} < B_{j+\frac{1}{2}}$ is treated similarly), this function is given by

$$\Psi_j(x) = \begin{cases} \widetilde{B}(x), & \text{if } x < x^*_j, \\ w_j, & \text{otherwise,} \end{cases}$$

where x_j^* is location of the wet/dry front in the cell C_j, which can be determined using the water mass conservation as follows:

$$\begin{aligned}\Delta x\cdot\overline{h}_j&=\int\limits_{x_{j-\frac12}}^{x_{j+\frac12}}\big(\Psi_j(x)-\widetilde{B}(x)\big)\,\mathrm{d}x=\int\limits_{x_j^*}^{x_{j+\frac12}}\big(w_j-\widetilde{B}(x)\big)\,\mathrm{d}x\\&=\frac{\Delta x_j^*}{2}\big(w_j-B_{j+\frac12}\big)=\frac{\Delta x_j^*}{2}\big(\widetilde{B}(x_j^*)-B_{j+\frac12}\big)=-\frac{(\Delta x_j^*)^2}{2}(B_x)_j,\end{aligned}\tag{3.1}$$

where $\Delta x_j^*:=x_{j+\frac12}-x_j^*$. It then follows from (3.1) that

$$x_j^*=x_{j+\frac12}-\Delta x\sqrt{\frac{2\overline{h}_j}{B_{j-\frac12}-B_{j+\frac12}}},\quad w_j=B_{j+\frac12}+\sqrt{2\overline{h}_j\big(B_{j-\frac12}-B_{j+\frac12}\big)}.\tag{3.2}$$

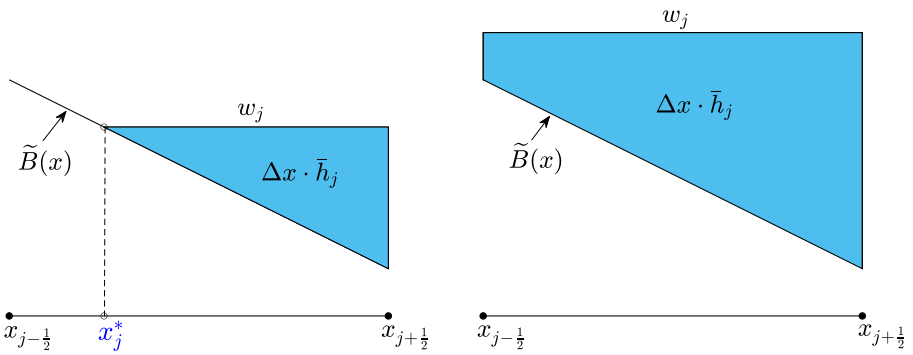

Figure 3.2: Computation of w_j in the partially (left) and fully (right) flooded cells.

We now consider a typical combined steady state with

$$\begin{aligned}&h_j=0,\quad\text{for } j<j_\ell-1\ \text{ or }\ j>j_r+1,\quad w_{j_\ell-1}=w_{j_\ell}=\cdots=w_{j_r}=w_{j_r+1}=\widehat{w},\\&\overline{q}_j=u_j\equiv0,\quad\text{for all } j,\end{aligned}\tag{3.3}$$

see Figure 3.1, and introduce a new approach for constructing the global flux variable, which will remain constant at such steady states. To this end, we first compute $R_{j+\frac12}$ for $j=j_\ell-1,\ldots,j_r$ using (2.6), R_{j_ℓ} using (2.15), and R_j for $j=j_\ell+1,\ldots,j_r$ using (2.16). As we have shown in §2.3, this will guarantee that $K_{j_\ell}=\cdots=K_{j_r}=\widehat{K}$ at the studied combined steady state. We will now need to develop formulae for computing $K_{j_\ell-1}$ and K_{j_r+1} satisfying the same property, namely, we need to ensure that at these states $K_{j_\ell-1}=K_{j_r+1}=\widehat{K}$ as well.

In order to achieve this goal, we notice that in all of the fully flooded cells,

$$w_j=\overline{h}_j+B_j,\quad j=j_\ell,\ldots,j_r.\tag{3.4}$$

However, in the partially flooded cells $C_{j_\ell-1}$ and C_{j_r+1}, (3.4) does not hold. Instead, one can show that

$$w_{j_\ell-1}=\overline{h}_{j_\ell-1}+\widehat{B}_{j_\ell-1},\quad w_{j_r+1}=\overline{h}_{j_r+1}+\widehat{B}_{j_r+1},\tag{3.5}$$

where $\widehat{B}_{j_\ell-1}$ is obtained using (3.2):

$$\widehat{B}_{j_\ell-1}=w_{j_\ell-1}-\overline{h}_{j_\ell-1}=B_{j_\ell-\frac{1}{2}}+\sqrt{2\,\overline{h}_{j_\ell-1}\big(B_{j_\ell-\frac{3}{2}}-B_{j_\ell-\frac{1}{2}}\big)}-\overline{h}_{j_\ell-1}. \tag{3.6}$$

Similarly, in cell C_{j_r+1}, we have

$$\widehat{B}_{j_r+1}=w_{j_r+1}-\overline{h}_{j_r+1}=B_{j_r+\frac{1}{2}}+\sqrt{2\,\overline{h}_{j_r+1}\big(B_{j_r+\frac{3}{2}}-B_{j_r+\frac{1}{2}}\big)}-\overline{h}_{j_r+1}. \tag{3.7}$$

Equipped with (3.6) and (3.7), we then set

$$\begin{aligned}
R_{j_\ell-1}&=R_{j_\ell}-\int\limits_{x_{j_\ell-1}}^{x_{j_\ell}}ghB_x\,\mathrm{d}x\approx R_{j_\ell}-\frac{g}{2}\big(\overline{h}_{j_\ell}+\overline{h}_{j_\ell-1}\big)\big(B_{j_\ell}-\widehat{B}_{j_\ell-1}\big),\\
R_{j_r+1}&=R_{j_r}+\int\limits_{x_{j_r}}^{x_{j_r+1}}ghB_x\,\mathrm{d}x\approx R_{j_r}+\frac{g}{2}\big(\overline{h}_{j_r}+\overline{h}_{j_r+1}\big)\big(\widehat{B}_{j_r+1}-B_{j_r}\big),
\end{aligned} \tag{3.8}$$

and hence using (2.8) we obtain

$$K_{j_\ell-1}=\frac{\overline{q}^2_{j_\ell-1}}{\overline{h}_{j_\ell-1}}+\frac{g}{2}\,\overline{h}^2_{j_\ell-1}+R_{j_\ell-1},\quad K_{j_r+1}=\frac{\overline{q}^2_{j_r+1}}{\overline{h}_{j_r+1}}+\frac{g}{2}\,\overline{h}^2_{j_r+1}+R_{j_r+1}. \tag{3.9}$$

Notice that this particular selection of the global variable values at the partially flooded cell $C_{j_\ell-1}$ guaranties that at the steady state (3.3), $K_{j_\ell-1}=K_{j_\ell}=\widehat{K}$. Indeed, substituting (3.3) into (3.8), (3.9) and using (3.4) and (3.5), we obtain

$$\begin{aligned}
K_{j_\ell}-K_{j_\ell-1}&=\frac{g}{2}\big(\overline{h}^2_{j_\ell}-\overline{h}^2_{j_\ell-1}\big)+R_{j_\ell}-R_{j_\ell-1}\\
&=\frac{g}{2}\big(\overline{h}_{j_\ell}+\overline{h}_{j_\ell-1}\big)\big(\overline{h}_{j_\ell}-\overline{h}_{j_\ell-1}+B_{j_\ell}-\widehat{B}_{j_\ell-1}\big)=\frac{g}{2}\big(\overline{h}_{j_\ell}+\overline{h}_{j_\ell-1}\big)\big(w_{j_\ell}-w_{j_\ell-1}\big)=0.
\end{aligned}$$

Similarly, one can show that at the steady state (3.3), $K_{j_r+1}=K_{j_r}=\widehat{K}$.

As it was mentioned in §1, we develop a hybrid approach, according to which the flux globalization based central-upwind scheme described in §2 will be used only inside the "wet" areas, namely, in cells $C_{j_\ell+1},\ldots,C_{j_r-1}$. Outside these areas, we will implement the scheme from [2], which is based on a special piecewise linear reconstruction of the water surface w. The resulting hybrid scheme will exactly preserve the aforementioned combined "lake-at-rest"–"dry lake" steady states provided the one-sided reconstructed point values coincide at the interfaces between these areas (these interfaces are marked by the red dashed line plotted in Figure 3.1). We therefore need to verify that at these steady states the following four equalities hold:

$$q^-_{j_\ell+\frac{1}{2}}=q^+_{j_\ell+\frac{1}{2}},\quad q^-_{j_r-\frac{1}{2}}=q^+_{j_r-\frac{1}{2}},\quad h^-_{j_\ell+\frac{1}{2}}=h^+_{j_\ell+\frac{1}{2}},\quad h^-_{j_r-\frac{1}{2}}=h^+_{j_r-\frac{1}{2}}. \tag{3.10}$$

The first two equalities immediately follow from the fact that $\overline{q}_j\equiv 0$ for all j and q is reconstructed in both schemes. Next, we prove the third equality in (3.10). Since we reconstruct w in cell C_{j_ℓ}, $w^-_{j_\ell+\frac{1}{2}}=w_{j_\ell}=\widehat{w}$ and we obtain

$$h^-_{j_\ell+\frac{1}{2}}=w^-_{j_\ell+\frac{1}{2}}-B_{j_\ell+\frac{1}{2}}=w_{j_\ell}-B_{j_\ell+\frac{1}{2}}\overset{(3.4)}{=}\overline{h}_{j_\ell}+B_{j_\ell}-B_{j_\ell+\frac{1}{2}}\overset{(2.1)}{=}\overline{h}_{j_\ell}-\frac{\Delta x}{2}(B_x)_{j_\ell}. \tag{3.11}$$

At the same time, we recontruct K in cell $C_{j_\ell+1}$, so that $K^+_{j_\ell+\frac12}=K_{j_\ell+1}=\widehat{K}$, and thus the right-sided value of h is

$$\begin{aligned}h^+_{j_\ell+\frac12}&=\sqrt{\frac{2}{g}(K^+_{j_\ell+\frac12}-R_{j_\ell+\frac12})}=\sqrt{\frac{2}{g}(K_{j_\ell}-R_{j_\ell+\frac12})}\overset{(2.8)}{=}\sqrt{\frac{2}{g}\Big(\frac{g}{2}\overline{h}^2_{j_\ell}+R_{j_\ell}-R_{j_\ell+\frac12}\Big)}\\&\overset{(2.6),\,(2.15)}{=\!=}\sqrt{\overline{h}^2_{j_\ell}+\Delta x(B_x)_{j_\ell}\Big(\overline{h}_{j_\ell}+\frac{\Delta x}{4}(B_x)_{j_\ell}\Big)-2\,\overline{h}_{j_\ell}\Delta x(B_x)_{j_\ell}}\\&=\sqrt{\Big(\overline{h}_{j_\ell}-\frac{\Delta x}{2}(B_x)_{j_\ell}\Big)^2}=\overline{h}_{j_\ell}-\frac{\Delta x}{2}(B_x)_{j_\ell}.\end{aligned}\tag{3.12}$$

As one can see, equations (3.11) and (3.12) imply $h^+_{j_\ell+\frac12}=h^-_{j_\ell+\frac12}$. The fourth equality in (3.10) can be verified analogously.

3.1 Hybrid Piecewise Linear Reconstruction: A Summary

We use two different piecewsie linear reconstructions in different parts of the computational domain.

• Inside the "wet" areas, that is, in the situation plotted in Figure 3.1 in cells $C_{j_\ell+1},\ldots,C_{j_r-1}$, as well as in the two remaining wet cells C_{j_ℓ} and C_{j_r}, we use the piecewise linear reconstructions of q and K, (2.10) and (2.11), to obtain $q^\pm_{j+\frac12}$ and $K^\pm_{j+\frac12}$ for $j=j_\ell,\ldots,j_r-1$. We then solve the cubic equations (2.12) and obtain the corresponding point values $h^\pm_{j+\frac12}$, $j=j_\ell,\ldots,j_r-1$.

• In the partially flooded and dry cells, that is, in the situation plotted in Figure 3.1 in cells C_j with $j\le j_\ell-1$ or $j\ge j_r+1$, as well as in the two wet cells C_{j_ℓ} and C_{j_r}, which have partially flooded or dry neighbors, we use the wet/dry reconstruction proposed in [2, Definition 3.2] and described below.

Given $\overline{h}_j$ and $\overline{q}_j$, we first compute the values $\overline{w}_j:=h_j+B_j$ and $u_j:=\overline{q}_j/\overline{h}_j$ (the latter computation needs to be desingularized as discussed in Remark 3.3 below) and perform a piecewise linear reconstruction similar to (2.10), (2.11), but for the fileds of w and u. We then use a formula similar to (2.9) to evaluate the one-sided point values of w and u, which we denote by $\widetilde{w}^\pm_{j+\frac12}$ and $u^\pm_{j+\frac12}$. The corresponding values of h are $\widetilde{h}^\pm_{j+\frac12}=\widetilde{w}^\pm_{j+\frac12}-B_{j+\frac12}$. Finally, the values of $h^\pm_{j+\frac12}$ and $w^\pm_{j+\frac12}$, which will be used in the numerical fluxes, are obtained by modifying $\widetilde{h}^\pm_{j+\frac12}$ and $\widetilde{w}^\pm_{j+\frac12}$ according to the following wet/dry correction algorithm.

Case 1 ($\overline{w}_j\ge B_{j-\frac12}$ and $\overline{w}_j\ge B_{j+\frac12}$): There is enough water in C_j to flood the entire cell.

Case 1A ($\widetilde{w}^+_{j-\frac12}\ge B_{j-\frac12}$ and $\widetilde{w}^-_{j+\frac12}\ge B_{j+\frac12}$): No correction is needed and we set

$$w^\pm_{j+\frac12}=\widetilde{w}^\pm_{j+\frac12},\quad h^\pm_{j+\frac12}=\widetilde{h}^\pm_{j+\frac12}.$$

Case 1B ($\widetilde{w}^+_{j-\frac12}<B_{j-\frac12}$ or $\widetilde{w}^-_{j+\frac12}<B_{j+\frac12}$): We correct the water surface slope and obtain

$$\begin{aligned}&\text{if }\ \widetilde{w}^-_{j+\frac12}<B_{j+\frac12},\quad\text{then we set }\ w^-_{j+\frac12}=B_{j+\frac12}\ \text{ and }\ w^+_{j-\frac12}=2\,\overline{w}_j-B_{j+\frac12};\\&\text{if }\ \widetilde{w}^+_{j-\frac12}<B_{j-\frac12},\quad\text{then se set }\ w^-_{j+\frac12}=2\,\overline{w}_j-B_{j-\frac12}\ \text{ and }\ w^+_{j-\frac12}=B_{j-\frac12}.\end{aligned}$$

Case 2 ($B_{j-\frac12} > \overline{w}_j > B_{j+\frac12}$): There might not be enough water in C_j to flood the entire cell.

Case 2A (the neighboring cell C_{j+1} satisfies Case 1A): We set

$$w^-_{j+\frac12} = w^+_{j+\frac12} \quad \text{and} \quad h^-_{j+\frac12} = w^-_{j+\frac12} - B_{j+\frac12}.$$

Case 2A1 ($2\overline{h}_j - h^-_{j+\frac12} \geq 0$): There is enough water in C_j to flood the entire cell and we set

$$h^+_{j-\frac12} = 2\overline{h}_j - h^-_{j+\frac12} \quad \text{and} \quad w^+_{j-\frac12} = h^+_{j-\frac12} + B_{j-\frac12}.$$

Case 2A2 ($2\overline{h}_j - h^-_{j+\frac12} < 0$): There is not enough water in C_j to flood the entire cell and we set

$$h^+_{j-\frac12} = 0 \quad \text{and} \quad w^+_{j-\frac12} = B_{j-\frac12}.$$

Notice that in this case the reconstruction within cell C_j consists of two linear pieces; see [2, Figure 5].

Case 2B (the neighboring cell C_{j+1} does not satisfy Case 1A): We set

$$w^-_{j+\frac12} = w_j \quad \text{and} \quad h^-_{j+\frac12} = w_j - B_{j+\frac12}$$

and consider Cases 2A1 and 2A2 to set the values $h^+_{j-\frac12}$ and $w^+_{j-\frac12}$.

Case 3 ($B_{j-\frac12} < \overline{w}_j < B_{j+\frac12}$): Analogous to Case 2.

Remark 3.1 *We stress that in the wet cells, which have partially flooded or dry neighbors, we roconstruct both q, K and u, w.*

3.2 Time Evolution of the Numerical Solution Inside and Outside the "Wet" Areas

In this section, we describe our hybrid well-balanced strategy of the time evolution of the numerical solution. Inside the "wet" areas, that is, in cells $C_{j_\ell+1}, \ldots, C_{j_r-1}$ in the situation illustrated in Figure 3.1, we use flux globalization based central-upwind evolution described in §2.1. Outside the "wet" areas, the solution is evolved according to the well-balanced central-upwind scheme from [2].

Remark 3.2 *It should be observed that at the cell interfaces $x_{j_\ell+\frac12}$ and $x_{j_r-\frac12}$ (in the situation shown in Figure 3.1), we compute the global central-upwind fluxes (2.5) and the central-upwind fluxes from [2] using the one-sided point values obtained from the two different reconstructions. However, this does not lead to any discrepancies since, as we have demonstrated in (3.10), in the case of the studied combined "lake-at-rest" and "dry lake" steady states, the left and right reconstructed point values will coincide at these two interfaces.*

Remark 3.3 *Inside the "wet" areas, we first reconstruct the one-sided point values $q^\pm_{j+\frac12}$ and then obtain the corresponding velocities (needed for the numerical flux evaluation) by taking $u^\pm_{j+\frac12} = q^\pm_{j+\frac12}/h^\pm_{j+\frac12}$. However, if the point values $h^\pm_{j+\frac12}$ become too small or zero, this calculation must be*

desingularized. To this end, we use the same desingularization technique as in [4, 7, 11], namely, we set

$$u^{\pm}_{j+\frac{1}{2}}=\frac{2\,h^{\pm}_{j+\frac{1}{2}}q^{\pm}_{j+\frac{1}{2}}}{\big(h^{\pm}_{j+\frac{1}{2}}\big)^2+\max\Big\{\big(h^{\pm}_{j+\frac{1}{2}}\big)^2,10^{-12}\Big\}}.$$

After that, for consistency we replace the point values $q^{\pm}_{j+\frac{1}{2}}$ and $K^{\pm}_{j+\frac{1}{2}}$ with the corrected values $h^{\pm}_{j+\frac{1}{2}}\cdot u^{\pm}_{j+\frac{1}{2}}$ and $h^{\pm}_{j+\frac{1}{2}}\cdot\big(u^{\pm}_{j+\frac{1}{2}}\big)^2+g\big(h^{\pm}_{j+\frac{1}{2}}\big)^2/2+R_{j+\frac{1}{2}}$, respecively.

Outside the "wet" areas, we reconstruct the one-sided point values $u^{\pm}_{j+\frac{1}{2}}$ and thus we first need to compute the point values $u_j=\overline{q}_j/\overline{h}_j$. This computation must be desingularized as well and hence we set

$$u_j=\frac{2\,\overline{h}_j\,\overline{q}_j}{\overline{h}_j^{\,2}+\max\Big\{\overline{h}_j^{\,2},10^{-12}\Big\}}.$$

Remark 3.4 *We stress that, while inside the "wet" areas we numerically integrate the Saint-Venant system (1.6) written using the global fluxes (1.7), outside the "wet" areas we numerically solve the Saint-Venant system written in the classical balance law form:*

$$\begin{cases}h_t+q_x=0,\\ q_t+\Big(hu^2+\dfrac{g}{2}h^2\Big)_x=-ghB_x.\end{cases}$$

Remark 3.5 *In order to ensure that the proposed scheme preserves the positivity of the water depth h, we implement the same "draining time step" technique, which was introduced in [3] and used in [2].*

3.3 Numerical Examples

In this section, we demonstrate the performance of the proposed hybrid well-balanced central-upwind scheme on two numerical examples.

In both of the examples, we take $g=9.8$ and use the free boundary conditions. We also use the same discretization of the cell averages of the initial conditions as in [2]. Assume that at time $t=0$ the states at cell interfaces $\boldsymbol{U}_{j+\frac{1}{2}}$ are given. We first use the trapezoidal rule to compute

$$\overline{q}_j=\frac{q_{j+\frac{1}{2}}+q_{j-\frac{1}{2}}}{2}.$$

We then follow [16] and distinguish between the following cases for the computation of the initial fluid depth cell averages:

- If both $h_{j-\frac{1}{2}}>0$ and $h_{j+\frac{1}{2}}>0$ or if $B_{j-\frac{1}{2}}=B_{j+\frac{1}{2}}$, then

$$\overline{h}_j=\frac{h_{j+\frac{1}{2}}+h_{j-\frac{1}{2}}}{2};$$

- If $\max\big\{h_{j-\frac{1}{2}},h_{j+\frac{1}{2}}\big\}>0$, $\min\big\{h_{j-\frac{1}{2}},h_{j+\frac{1}{2}}\big\}=0$, and $B_{j-\frac{1}{2}}\neq B_{j+\frac{1}{2}}$, then

$$\overline{h}_j=\frac{\max\big\{h^2_{j-\frac{1}{2}},h^2_{j+\frac{1}{2}}\big\}}{2\big|B_{j-\frac{1}{2}}-B_{j+\frac{1}{2}}\big|}.$$

Example 3—Combined "Lake-at-Rest" and "Dry Lake" Steady State

In this numerical example, we consider the following steady state:

$$h_{\rm eq}(x)=\max\big\{0,0.4-B(x)\big\},\quad u_{\rm eq}(x)\equiv 0, \tag{3.13}$$

with a nonflat bottom topography containing two humps and defined by

$$B(x)=\begin{cases}0.2-0.2(x-7)^2, & \text{if } 6\le x\le 8,\\ 0.48-0.12(x-17)^2, & \text{if } 15\le x\le 19,\\ 0, & \text{otherwise,}\end{cases} \tag{3.14}$$

as illustrated in Figure 3.3. As one can see, the lower hump is completely submerged, whereas the higher hump is only partially submerged.

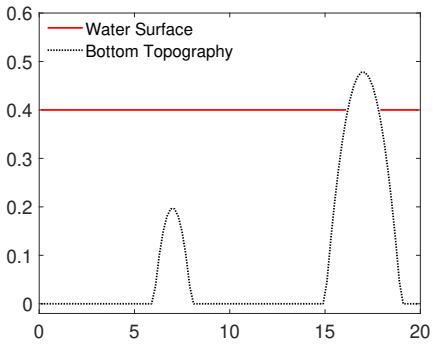

Figure 3.3: Example 3: Combined "lake-at-rest" and "dry lake" steady state (3.13).

We first take the computational domain $[0,20]$ and use (3.13), (3.14) as the initial conditions. The obtained results clearly show that the combined steady state (3.13), (3.14) is preserved by the proposed hybrid scheme within the machine accuracy.

We then superimpose a small perturbation onto the background (3.13), that is, we take the following initial data:

$$h(x,0)=h_{\rm eq}(x)+\begin{cases}10^{-4}, & \text{if } 11\le x\le 12,\\ 0, & \text{otherwise,}\end{cases}\qquad u(x,0)\equiv 0.$$

We compute the numerical solution by the proposed hybrid scheme until the final time $t=4.2$ using 400 uniform cells. In Figure 3.4, we plot the difference $h(x,t)-h_{\rm eq}(x)$ at different times. As expected, the perturbation splits into two waves propagating in the opposite directions ($t=0.6$). At time $t=1.8$, the left-going wave is located over the lower hump ($x\in[6,8]$) and its magnitude increases. Moreover, one can see that a small reflected wave is generated and moves to the right. At time $t=2.4$, the left-going wave passes the hump and its magnitude decreases to the original level. At the same time, the right-going wave reaches the higher hump located in $[15,19]$. After that, the left-going wave keeps moving and its shape does not change much. However, the right-going wave starts interacting with the higher hump. At time $t=3$, the right-going wave passes over the submerged part of the higher hump and the magnitude of the wave increases. At the same time, a small reflected wave is generated and starts propagating to the left. At time $t=3.6$,

the right-going wave propagates over the initially dry part of the hump and the magnitude of the wave keeps increasing. Finally, at time $t = 4.2$, the water flows down the hump and magnitude of the right-going perturbation decreases.

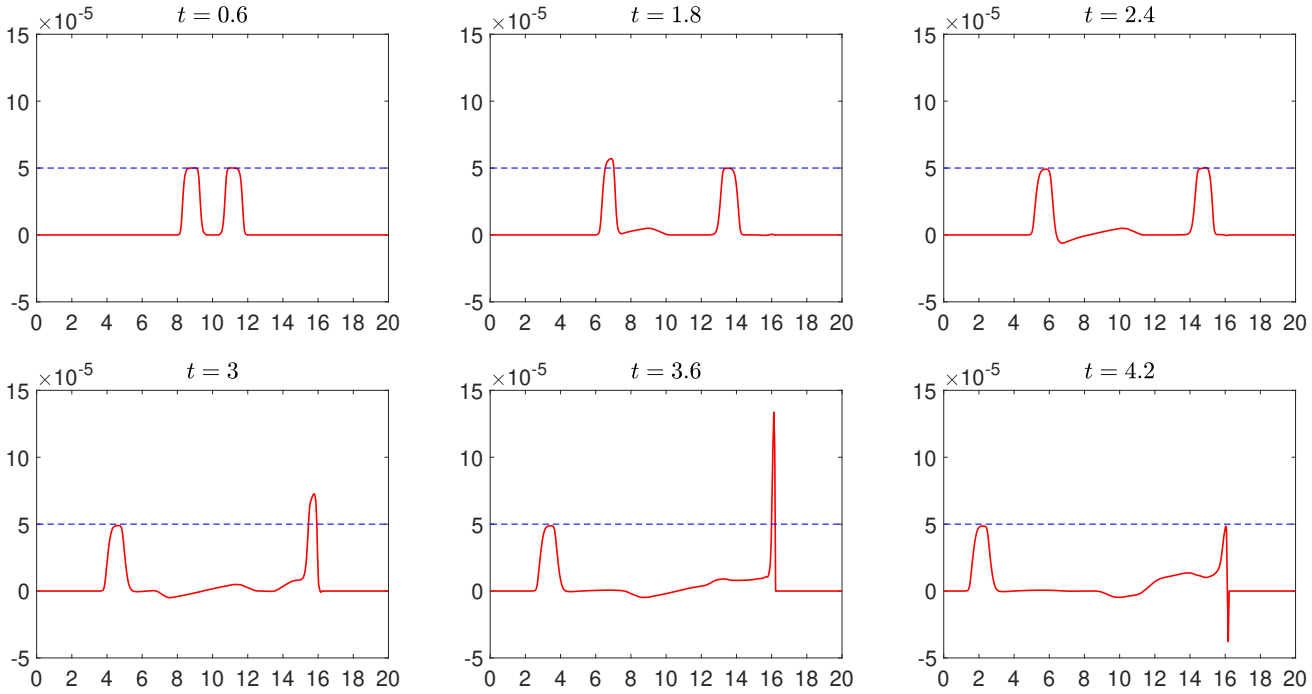

Figure 3.4: Example 3: Time snapshots of $h(x,t) - h_{\rm eq}(x)$ computed by the proposed hybrid scheme. Blue dashed line is a horizontal line at the level $5 \cdot 10^{-5}$.

Remark 3.6 *We note that in this example, we have used two sets of global variables: one of them has been used on the left of the "dry" area located on the top of the higher hump, and the second set of global variables has been used on the right of that "dry" area.*

Example 4—Still and Oscillating Lakes with Wet/Dry Fronts

In the final example taken from [1] (also studied in [2]), we consider the still and oscillating lakes in a parabolic basin described by the following bottom topography function:

$$B(x) = \frac{1}{4}\left[1 - \cos\big((2x-1)\pi\big)\right]. \tag{3.15}$$

The still lake equilibrium is given by

$$h_{\rm eq}(x) = \max\big\{0, 0.4 - B(x)\big\}, \quad u_{\rm eq}(x) \equiv 0, \tag{3.16}$$

which corresponds to a combined "lake-at-rest" and "dry lake" steady state.

We first take the computational domain $[0,1]$ and use (3.16), (3.15) as the initial conditions. The obtained results clearly show that the combined steady state (3.16), (3.15) is preserved by the proposed hybrid scheme within the machine accuracy, as expected.

We then introduce a sinusoidal perturbation of h_{eq} and take the following initial data:

$$h(x,0)=\max\left\{0,0.4+\frac{\sin\left(4x-2-\max\left\{0,-0.4+B(x)\right\}\right)}{25}-B(x)\right\}.$$

In Figure 3.5, we plot the water surface w and discharge q at the final time $t=19.87$ computed by the proposed hybrid scheme using 200 uniform cells. The ontained results are compared with a reference solution computed by the scheme from [2] on a very fine mesh with 12800 cells. As one can see, the proposed hybrid scheme provides an accurate approximation of wet/dry fronts without producing any spurious waves during the wetting and drying processes.

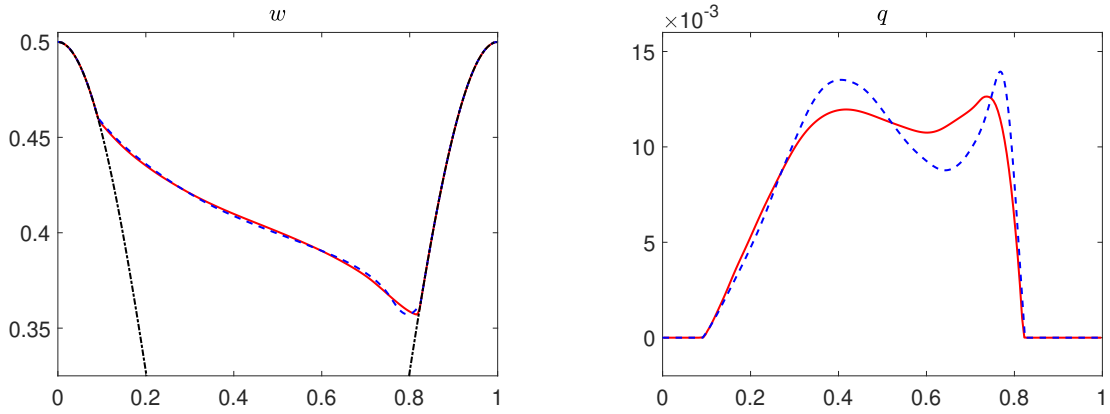

Figure 3.5: Example 4 (oscillating lake): Water surface w together with the bottom topography B (left) and discharge q (right). Red solid lines represent the results by the proposed hybrid scheme, blue dashed lines represent the reference solution, and black dash-dotted lines stand for the bottom topography.

Declarations:

Funding. The work of A. Chertock was supported in part by NSF grant DMS-1818684. The work of A. Kurganov was supported in part by NSFC grants 11771201 and 1201101343, and by the fund of the Guangdong Provincial Key Laboratory of Computational Science and Material Design (No. 2019B030301001).

Conflicts of interest. On behalf of all authors, the corresponding author states that there is no conflict of interest.

Data and software availability. The data that support the findings of this study and FORTRAN codes developed by the authors and used to obtain all of the presented numerical results are available from the corresponding author upon reasonable request.

References

[1] E. Audusse, F. Bouchut, M.-O. Bristeau, R. Klein, and B. Perthame, *A fast and stable well-balanced scheme with hydrostatic reconstruction for shallow water flows*, SIAM J. Sci. Comput., 25 (2004), pp. 2050–2065.

[2] A. Bollermann, G. Chen, A. Kurganov, and S. Noelle, *A well-balanced reconstruction of wet/dry fronts for the shallow water equations*, J. Sci. Comput., 56 (2013), pp. 267–290.

[3] A. Bollermann, S. Noelle, and M. Lukáčová-Medviďová, *Finite volume evolution Galerkin methods for the shallow water equations with dry beds*, Commun. Comput. Phys., 10 (2011), pp. 371–404.

[4] Y. Cheng, A. Chertock, M. Herty, A. Kurganov, and T. Wu, *A new approach for designing moving-water equilibria preserving schemes for the shallow water equations*, J. Sci. Comput., 80 (2019), pp. 538–554.

[5] A. Chertock, S. Cui, A. Kurganov, Ş. N. Özcan, and E. Tadmor, *Well-balanced schemes for the Euler equations with gravitation: Conservative formulation using global fluxes*, J. Comput. Phys., 358 (2018), pp. 36–52.

[6] A. Chertock, M. Herty, and Ş. N. Özcan, *Well-balanced central-upwind schemes for* 2×2 *systems of balance laws*, in Theory, Numerics and Applications of Hyperbolic Problems I, vol. 236 of Springer Proceedings in Mathematics & Statistics, Springer, 2018, pp. 345–361.

[7] A. Chertock, A. Kurganov, and Y. Liu, *Central-upwind schemes for the system of shallow water equations with horizontal temperature gradients*, Numer. Math., 127 (2014), pp. 595–639.

[8] S. Gottlieb, D. Ketcheson, and C.-W. Shu, *Strong stability preserving Runge-Kutta and multistep time discretizations*, World Scientific Publishing Co. Pte. Ltd., Hackensack, NJ, 2011.

[9] S. Gottlieb, C.-W. Shu, and E. Tadmor, *Strong stability-preserving high-order time discretization methods*, SIAM Rev., 43 (2001), pp. 89–112.

[10] A. Kurganov and C.-T. Lin, *On the reduction of numerical dissipation in central-upwind schemes*, Commun. Comput. Phys., 2 (2007), pp. 141–163.

[11] A. Kurganov, Y. Liu, and V. Zeitlin, *A well-balanced central-upwind scheme for the thermal rotating shallow water equations*, J. Comput. Phys., 411 (2020), p. 109414.

[12] ——, *Thermal vs isothermal rotating shallow water equations: Comparison of dynamical processes in two models by simulations with a novel well-balanced central-upwind scheme*, Geophys. Astrophys. Fluid Dyn., 115 (2021), pp. 125–154.

[13] A. Kurganov and G. Petrova, *A second-order well-balanced positivity preserving central-upwind scheme for the Saint-Venant system*, Commun. Math. Sci., 5 (2007), pp. 133–160.

[14] X. Liu, X. Chen, S. Jin, A. Kurganov, and H. Yu, *Moving-water equilibria preserving partial relaxation scheme for the Saint-Venant system*, SIAM J. Sci. Comput., 42 (2020), pp. A2206–A2229.

[15] H. Nessyahu and E. Tadmor, *Nonoscillatory central differencing for hyperbolic conservation laws*, J. Comput. Phys., 87 (1990), pp. 408–463.

[16] M. Ricchiuto and A. Bollermann, *Stabilized residual distribution for shallow water simulations*, J. Comput. Phys., 228 (2009), pp. 1071–1115.

[17] P. K. Sweby, *High resolution schemes using flux limiters for hyperbolic conservation laws*, SIAM J. Numer. Anal., 21 (1984), pp. 995–1011.

[18] B. van Leer, *Towards the ultimate conservative difference scheme. V. A second-order sequel to Godunov's method*, J. Comput. Phys., 32 (1979), pp. 101–136.